Scaling of temperature- and stress-dependent viscosity convection

V. S. Solomatov

Seismological Laboratory, 252-21, California Institute of Technology, Pasadena, California 91125

Simple scaling analysis of temperature- and stress-dependent viscosity convection with free-slip boundaries suggests three convective regimes: the small viscosity contrast regime which is similar to convection in a fluid whose viscosity does not depend on temperature, the transitional regime characterized by self-controlled dynamics of the cold boundary layer and the asymptotic regime in which the cold boundary becomes stagnant and convection involves only the hottest part of the lid determined by a rheological temperature scale. The first two regimes are usually observed in numerical experiments. The last regime is similar to strongly temperature-dependent viscosity convection with rigid boundaries studied in laboratory experiments. © *1995 American Institute of Physics.*

I. INTRODUCTION

Studying of a developed high Prandtl number convection in temperature- and stress-dependent viscosity fluids has been started a long time ago with applications to the Earth's mantle.[1-11] Systematic studies done during the last decade provide a sufficient basis for development of a physical model of variable viscosity convection. Christensen[12-14] investigated 2-D temperature-, pressure- and stress-dependent viscosity convection. Hansen and Yuen[15] studied temperature-dependent viscosity convection at higher Rayleigh numbers. Numerical models of 3-D convection with temperature-dependent viscosity also becomes more systematic; see, for example, Ogawa et al.[16]

Extensive laboratory experiments on temperature-dependent viscosity convection with rigid boundaries were performed recently by Davaille and Jaupart[17] who suggested scaling relations for the heat transport and found a qualitative agreement with asymptotic boundary layer theories developed by Morris and Canright[18] and Fowler.[19] However, in contrast to the predictions of boundary layer theories, convection with free boundaries seems to behave differently and obey different laws.[12-16,20] A simple physical analysis presented in this paper suggests that with increase of the viscosity contrasts, temperature-dependent viscosity convection passes through a substantial period of transitional regimes before it enters the asymptotic regime described by Morris and Canright[18] and Fowler.[19] The theory reconciles and systematizes various numerical, laboratory, and analytical results and suggests scaling relations for all convective regimes. The paper starts with Newtonian viscosity and then the scaling relations are generalized for non-Newtonian viscosity fluids.

II. ENERGETICS OF CONVECTION

Consider a steady-state Rayleigh-Benard convection in a cell with approximately equal horizontal and vertical dimensions and with a fixed temperature difference ΔT between the boundaries. This convective cell is assumed to be a part of a periodic structure of an infinite horizontal layer. The equations of steady-state thermal convection with Boussinesq approximation and with infinite Prandtl number are (e.g., Refs. 1 and 6):

$$\frac{\partial p}{\partial x_i} = \alpha \rho g \lambda_i T + \frac{\partial \tau_{ij}}{\partial x_j}, \tag{1}$$

$$u_i \frac{\partial T}{\partial x_i} = \kappa \frac{\partial^2 T}{\partial x_j^2}, \tag{2}$$

$$\frac{\partial u_i}{\partial x_i} = 0, \tag{3}$$

where x_i are the coordinates, u_i is the velocity, p and T are the pressure and temperature perturbations, α is the thermal expansion, g is the acceleration due to gravity, λ_i is a unit vector in the direction of gravity, $\kappa = k/\rho c_p$ is the coefficient of thermal diffusion, ρ is the density, k is the thermal conductivity, c_p is the heat capacity at constant pressure,

$$\tau_{ij} = \eta \dot{e}_{ij} = \eta \left(\frac{\partial u_i}{\partial x_j} + \frac{\partial u_j}{\partial x_i} \right) \tag{4}$$

is the deviatoric stress tensor, $\dot{e}_{ij}$ is the strain rate tensor, and η is the viscosity. The surface temperature is $T_0 = 0$, the bottom temperature is $T_1 = \Delta T$. All boundaries are free-slip.

The scaling analysis will use the fact that whatever viscosity law is considered and whatever is the distribution of viscous dissipation in the layer, the integral viscous dissipation Φ_{diss} in the layer is always balanced by the integral mechanical work done by thermal convection per unit time:[21]

$$\Phi_{\text{diss}} = \int_V \tau_{ij} \frac{\partial u_i}{\partial x_j} \, dV = \frac{\alpha g d}{c_p} FS \left(1 - \frac{1}{\text{Nu}} \right) \approx \frac{\alpha g V}{c_p} F, \tag{5}$$

where V is the volume and S is the surface area of the layer, F is the heat flux, and Nu is the Nusselt number:

$$\text{Nu} = \frac{dF}{k\Delta T}. \tag{6}$$

The second part of (5) is valid if $\text{Nu} \gg 1$.

The energetic constraint (5), assumptions about the dissipational structure and the thermal boundary layer relations will be used to find the scaling laws.

III. SMALL VISCOSITY CONTRAST CONVECTION

Suppose that the viscosity is Newtonian:

$$\eta = \eta_0 \exp(-\gamma T), \tag{7}$$

where η_0 is the viscosity at the cold surface, where $T = 0$ and γ is a constant. Such a simple exponential function is the most studied viscosity law. It requires only one non-dimensional parameter, for example,

$$p = \gamma \Delta T \tag{8}$$

in addition to the Rayleigh number used for constant viscosity convection.

If the viscosity contrast is small, convection is similar to constant viscosity convection: the flow is uniform and the energy balance (5) can be written as

$$\eta_i \left(\frac{u_0}{d} \right)^2 V \sim \frac{\alpha g F}{c_p} V, \tag{9}$$

where d is the layer thickness, u_0 is the amplitude velocity, u_0/d is the characteristic strain rate scale and the viscosity

$$\eta_i = \eta_0 \exp(-\gamma T_i), \tag{10}$$

calculated at the interior temperature $T_i \approx \Delta T/2$ is the viscosity at which the most of viscous dissipation takes place. This evaluation of the dissipation integral is based on the largest scale of motion, meaning that a single Fourier mode is employed.

The flow is approximately symmetric relative to the horizontal axis through the center of the cell, so that the horizontal velocity u_0 near the upper boundary is approximately equal to the horizontal velocity u_1 near the lower boundary. The temperature drop ΔT across the layer is concentrated in two thermal boundary layers of approximately equal thicknesses:

$$\delta_0 \sim \delta_1 \sim \left(\frac{\kappa d}{u_0} \right)^{1/2}, \tag{11}$$

and the heat flux is

$$F \sim k \frac{\Delta T}{\delta_0}. \tag{12}$$

We obtain

$$\delta_0 \sim \delta_1 \sim d \, \mathrm{Ra}_i^{-1/3}, \quad \mathrm{Nu} \sim d/\delta_0, \tag{13}$$

$$u_0 \sim u_1 \sim \kappa d/\delta_0^2, \tag{14}$$

which are similar to relations for constant viscosity convection (e.g., Ref. 22) with the Rayleigh number defined at the interior viscosity η_i:

$$\mathrm{Ra}_i = \frac{\alpha g \rho \Delta T d^3}{\kappa \eta_i}. \tag{15}$$

IV. TRANSITIONAL REGIME

If the viscosity contrast is large, dissipation in the cold boundary layer becomes comparable with the dissipation in the internal region. In other words, the resistance to the motion of the cold boundary layer due to the deformation of the

cold boundary layer itself becomes comparable with the viscous drag of the interior region. A self-controlled cold boundary layer dynamics characterized by an approximate balance between the viscous dissipation in the cold thermal boundary layer and the work done by its negative buoyancy can take place in some parameter range.

To estimate this balance, we assume that the largest resistance to the motion of the cold boundary layer is in the bend of the cold boundary layer (where it starts sinking) and that the stresses due to the underlying low viscosity fluid can be ignored. This region has an area of the order of δ_0^2. The length scale of the velocity change there is of the order of δ_0, so that the strain rate is of the order of u_0/δ_0 (ignoring a weak dependence on a logarithmically varying parameter p).

The energy balance is now written as

$$\eta_0 \left(\frac{u_0}{\delta_0} \right)^2 \delta_0^2 l \sim \frac{1}{2} \frac{\alpha g F}{c_p} V, \tag{16}$$

where l is the horizontal size in the direction perpendicular to the direction of motion, so that $V = d^2 l$, and the coefficient $1/2$ indicates that the work done by the negative buoyancy of the cold boundary layer contributes approximately $1/2$ to the total energy balance.[20,21]

The other half of the convective work is done by the hot thermal boundary layer. An almost isothermal flow in the internal region is driven by approximately the same work per unit time and dissipates approximately the same amount of energy per unit time. It has the length scale d and the strain rate scale u_1/d, where u_1 is now the characteristic velocity in the internal region. Thus, the energy balance for this region is similar to that for the small viscosity contrast regime:

$$\eta_i \left(\frac{u_1}{d} \right)^2 V \sim \frac{1}{2} \frac{\alpha g F}{c_p} V. \tag{17}$$

The boundary layer relations depend on characteristic velocities at the boundaries which are now different for the upper and lower boundary:

$$\delta_0 \sim \left(\frac{\kappa d}{u_0} \right)^{1/2}, \quad \delta_1 \sim \left(\frac{\kappa d}{u_1} \right)^{1/2}. \tag{18}$$

Together with energetic equations and with the assumption that $\delta_0 \gg \delta_1$ they give

$$\delta_0 \sim d \mathrm{Ra}_0^{-1/3}, \quad \delta_1 \sim d \mathrm{Ra}_0^{-1/12} \mathrm{Ra}_i^{-1/4}, \tag{19}$$

where Ra_0 is defined at the surface viscosity:

$$\mathrm{Ra}_0 = \frac{\alpha g \rho \Delta T d^3}{\kappa \eta_0}. \tag{20}$$

The Nusselt number and the interior temperature are

$$\mathrm{Nu} \approx d/(\delta_0 + \delta_1); \quad T_i \approx \Delta T \delta_0/(\delta_0 + \delta_1). \tag{21}$$

V. STAGNANT LID REGIME

In the limit of very large viscosity contrasts, the advective heat transport due to the motion of the cold boundary layer becomes negligible compared to the heat transport due to a much faster convection beneath it. An effectively stagnant lid is developed on the top of the convective layer.

Phys. Fluids, Vol. 7, No. 2, February 1995

V. S. Solomatov   267

A linear temperature distribution in the lid results in an exponential growth of the viscosity when approaching the surface. Because the stresses τ_0 in the lid vary insignificantly, the strain rate also decays exponentially with the distance Δz from the bottom of the lid:

$$\dot{e} \sim \tau_0 \eta^{-1} \sim \tau_0 \eta_i^{-1} \exp(-\gamma \nabla T \Delta z), \qquad (22)$$

where $\nabla T \sim \Delta T / \delta_0$ is the temperature gradient in the cold boundary layer and the total temperature difference ΔT through the convective layer is taken as the temperature drop scale in the cold boundary layer.

As a result, convection penetrates into the cold lid only by a small length determined by the exponential decay constant:

$$\delta_{\mathrm{rh}} \sim \frac{\delta_0}{\gamma \Delta T} = \frac{\delta_0}{p} . \qquad (23)$$

The temperature difference which drives the convective flow is proportional to the rheological temperature difference scale

$$\Delta T_{\mathrm{rh}} \sim \gamma^{-1} = p^{-1} \Delta T. \qquad (24)$$

Convection beneath the lid is reduced to a constant viscosity convection with an effective driving temperature difference scale (24). This gives

$$\delta_0 \sim dp^{4/3} \mathrm{Ra}_i^{-1/3}, \qquad \delta_1 \sim p^{-1} \delta_0, \qquad \mathrm{Nu} \sim d/\delta_0. \qquad (25)$$

The thickness of the thermal boundary layer can be constrained independently with the help of assumption that the thermal boundary layer is at the margin of convective stability (see, e.g., Busse[23]). For asymptotically large viscosity contrasts, the critical Rayleigh number is equal to:[24]

$$\mathrm{Ra}_{1,\mathrm{cr}} = 20.9 \, p^4, \qquad (26)$$

where index "1" denotes the Rayleigh number defined at the viscosity of the bottom.

Applying this criterion to the cold boundary layer we require

$$\frac{\alpha g \rho \Delta T \delta_0^3}{\kappa \eta_i} = \mathrm{Ra}_{1,\mathrm{cr}}, \qquad (27)$$

where η_i is used as the viscosity of the bottom of the boundary layer and thus

$$\delta_0 \sim dp^{4/3} \mathrm{Ra}_i^{-1/3}, \qquad (28)$$

which coincides with (25).

Note, that instability occurs not in the entire boundary layer but only in a thin sublayer near the bottom, provided $e^p > e^8 \approx 3 \times 10^3$. The thickness of the unstable sublayer is equal to[24]

$$z_{\mathrm{sub}} = \frac{8 \delta_0}{p} . \qquad (29)$$

The scale δ_0/p characterizes the thickness of the thermal boundary layers in the active part of the convective cell, $\delta_1 \sim \delta_0/p$, and is in agreement with (23) and (25).
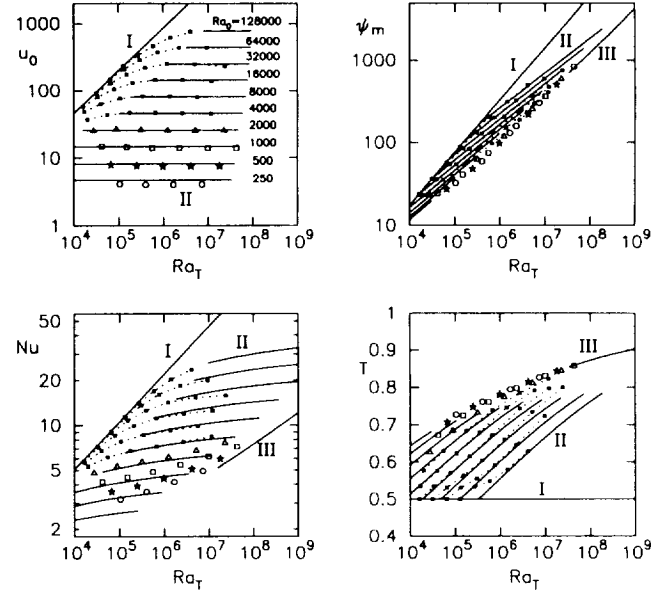

FIG. 1. The fitting curves (solid lines) describing Newtonian temperature-dependent viscosity convection are compared with numerical data. The averaged surface velocity u_0, the Nusselt number Nu, the maximum of stream-function ψ_m, and the average temperature T are shown as functions of Ra_T. The Rayleigh number Ra_0 is fixed for each curve, so that the viscosity contrast increases along each curve. Christensen's[13] numerical results for $\mathrm{Ra}_0 = 4000$, 8000, 16000, 32000, 64000, 128000 are shown with solid boxes connected with dotted lines. The data for $\mathrm{Ra}_0 = 250,500,1000,2000$ are shown with different symbols. The convective regimes indicated are: I—the small viscosity contrast regime, II—the transitional regime, and III—the stagnant lid regime. In the third regime, all theoretical curves are very close to each other and only one asymptotic curve is shown.

VI. COMPARISON WITH EXPERIMENTS

To compare the scaling laws with numerical and laboratory experiments, the formulae are non-dimensionalized using d for the length scale, k/d for the velocity scale, and ΔT for the temperature scale. This comparison is sometimes problematic because the data are plotted with the help of different non-dimensional numbers. The Rayleigh number Ra_T based on the viscosity calculated at the volumetrically averaged temperature $\bar{T}$ and the Rayleigh number Ra_0 were used by Christensen[12-14] and Hansen and Yuen.[15] The theoretical curves can be presented in terms of $\bar{T}$ and Ra_T instead of T_i and Ra_i using an approximate relation between $\bar{T}$ and T_i:

$$\bar{T} \approx T_i + (0.5 T_i^{-1} - 1) \delta_0. \qquad (30)$$

This assumes a linear temperature distribution in thermal boundary layers.

The correction for the difference between Ra_T and Ra_i is important for the temperature and for the maximum of streamfunction because they both strongly depend on T_i. The surface velocity and Nusselt number are not influenced by this correction.

The fit to Christensen's[13] data (the surface velocity, the Nusselt number, the maximum of streamfunction, and the average temperature) with the help of the theoretical dependences is shown in Fig. 1. The fitting formulae are compared with the theoretical ones in Table I. The maximum of stream-

TABLE I. Theory versus experiments: Newtonian viscosity.

Parameter	Theory	Fit
I. Small viscosity contrast regime		
δ_0	$\sim Ra_i^{0.333}$	$1.85\ Ra_i^{-0.3185}$
δ_1	$\sim \delta_0$	δ_0
u_0	$\sim \delta_0^{-2}$	$0.445\delta_0^{-2}$
ψ_m	$\sim \delta_1^{-2}$	$0.171\delta_1^{-2}$
II. Transitional regime		
δ_0	$\sim Ra_0^{-0.333}$	$3.2\ Ra_0^{-0.41}$
δ_1	$\sim Ra_0^{0.083}\ Ra_i^{-0.25}$	$1.524\ Ra_0^{-0.12}Ra_i^{-0.21}$
u_0	$\sim \delta_0^{-2}$	$0.52\delta_0^{-2}$
ψ_m	$\sim \delta_1^{-2}$	$0.11\delta_1^{-2}$
III. Stagnant lid regime[a]		
δ_0	$\sim p^{1.333}\ Ra_i^{-0.333}$	$1.85p^{1.3185}Ra_i^{-0.3185}$
δ_1	$\sim p^{-1}\delta_0$	$p^{-1}\delta_0$
ψ_m	$\sim \delta_1^{-2}$	$0.11\delta_1^{-2}$
All regimes		
Nu	$(\delta_0+\delta_1)^{-1}$	$(\delta_0+\delta_1)^{-1}$
T	$(1+\delta_1/\delta_0)^{-1}$	$(1+\delta_1/\delta_0)^{-1}$

[a]The fitting coefficients are poorly constrained.

FIG. 2. The fitting curves are plotted together with numerical and experimental data (divided for convenience into two figures) from Christensen[13] (the same as in Fig. 1), Ogawa et al.[16] (triangles, $Ra_0=10^3$), Hansen and Yuen[15] (solid circles, $Ra_0=10^4,10^5,10^6,10^7,10^8$). The curve corresponding to the scaling law suggested by Davaille and Jaupart[17] for convection with rigid boundaries is shown with a heavy solid line. A bifurcation-like transition from whole-layer to stagnant lid convection observed by Ogawa et al.[16] is marked with an open circle (it is shown in other coordinates as well, Fig. 3).

function calculated by Christensen[13] is approximately proportional to the velocity near the bottom (the most active region):

$$\psi_m \sim u_1. \tag{31}$$

Figure 2 shows the theoretical curves and the data from Christensen,[13] Ogawa et al.[16] (3-D calculations), and Hansen and Yuen.[15] The scaling law suggested by Davaille and Jaupart[17] for convection with rigid boundaries and a bifurcation observed by Ogawa et al.[16] are also shown.

This comparison shows that the stagnant lid regime is similar to convection with rigid boundaries and the numerical curves asymptotically approach this regime. On the other hand, the transitional regime in convection with rigid boundaries is much shorter as indicated by the experiments.[17] This is probably because the motion of the cold boundary layer has a larger drag over the entire upper boundary and convection enters the stagnant lid regime at smaller viscosity contrasts.

A qualitative agreement between the data from Ogawa et al.[16] and the corresponding theoretical curve plotted in the axes used by Ogawa et al.[16] supports the suggestion that the bifurcation observed by Ogawa et al.[16] is located at the boundary between the transitional and stagnant lid regime (Fig. 3).

The convective regimes are summarized in Fig. 4. The boundaries between the regimes are plotted in terms of the Rayleigh number Ra_1, based on the bottom viscosity η_1, and the viscosity contrast $\eta_0/\eta_1 = \exp(p)$. These coordinates allow to plot also the stability curve. To transform Ra_i to Ra_1, we use the fact that in small viscosity contrast regime $Ra_i \approx Ra_1 \exp(p/2)$. In the stagnant lid regime, the viscosity drop across the lower thermal boundary layer is a constant,[18,19,25] which is approximately equal to 4, so that $Ra_i \approx Ra_1/4$ and the viscosity drop across the lower boundary layer is $\exp(p)/4$.
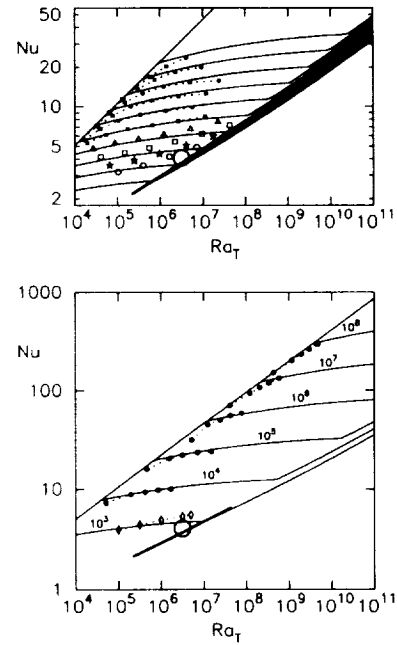
The boundary between small viscosity contrast regime and transitional regime is determined by the condition that the resistance of the cold boundary layer to its motion becomes comparable with the resistance of the interior region. This boundary can be defined with the help of intersection of the curves for these two regimes.
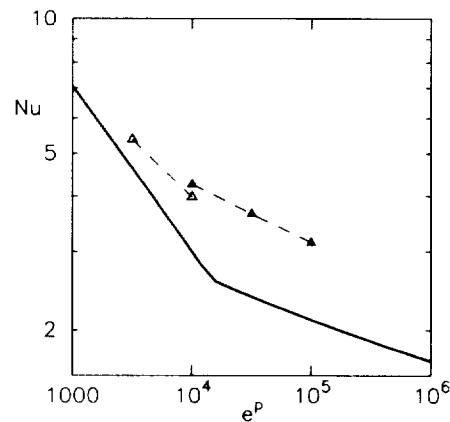

FIG. 3. The data showing the transition from whole-layer to stagnant lid convection (open and solid triangles respectively)[16] are plotted in the coordinates used by Ogawa et al.:[16] Nusselt number versus the viscosity contrast $\exp(p)$. The Rayleigh number $Ra_1 = 3.2\times10^6$ based on the viscosity of the bottom is fixed. The corresponding theoretical curve is shown with a solid line.

Phys. Fluids, Vol. 7, No. 2, February 1995
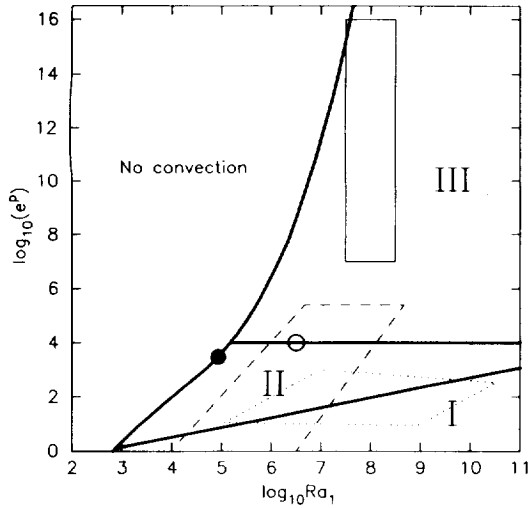
V. S. Solomatov   269

FIG. 4. The three convective regimes are shown in $Ra_1 - \exp(p)$ axes: I—the small viscosity contrast regime, II— the transitional regime, and III—the stagnant lid regime. The boundary between transitional and stagnant lid regimes is determined by the instability mode change in the cold boundary layer. The boundary for the onset of convection is also shown. The large solid circle separates the stability curve by a lower part where instability occurs in the entire layer and an upper part where instability occurs in the sublayer. Approximate parameter ranges studied in the numerical experiments are indicated (Christensen[13]—dashed contour, Hansen and Yuen[15]—dotted contour, and the bifurcation-like transition observed by Ogawa et al.[16] is shown with an open circle). A formal location of the Earth's mantle is shown with a solid contour assuming $\eta_i = 10^{22}$ P (Ref. 33). Because the viscosity of the mantle obeys the Arrhenius law, not the exponential one, the parameter p is calculated as $p = E\Delta T/(RT_i^2)$ for the range of activation energies E corresponding to different creep mechanisms.[34] A formal viscosity contrast across the lithospheric plates would be many orders of magnitude larger provided the viscosity law could be extrapolated up to the surface.

The boundary between the transitional regime and the asymptotic regime is more uncertain. It could be determined by the condition that the conductive heat transport through the lid becomes comparable with the advective heat transport due to the motion of the lid. However, such a formal calculation does not take into account a change in the instability mode in the cold boundary layer, from instability in the entire thermal boundary layer to instability in the sublayer. The change in the instability mode causes a stagnation of the uppermost part of the cold boundary layer and as a result, an earlier transition to the stagnant lid regime. The alternative boundary between the transitional regime and the stagnant lid regime is determined by the condition that the viscosity contrast in the cold boundary layer is equal to the critical value, $\exp(8) \sim 3 \times 10^3$ (this is the boundary shown in Fig. 4). This boundary passes precisely through the bifurcation observed by Ogawa et al.[16] This implies that in the bifurcation point, the viscosity contrast across the cold boundary layer must be equal to the critical one ($\sim 3 \times 10^3$) and the rest of the viscosity drop (a factor of 3–4) must be in the bottom boundary layer. This is in agreement with Ogawa et al.'s[16] data. A transition resembling the transition to stagnant lid regime was also observed in previous works on linear and mean-field temperature-dependent viscosity convection.[26–28]

The critical viscosity contrasts reported are close to the value indicated above.

The scaling relations obtained can be compared with the predictions of boundary layer theories developed by Morris and Canright[21] and Fowler[22] for the stagnant lid regime. Qualitatively they suggest similar results. However, they predict somewhat weaker dependence of the Nusselt number on the Rayleigh number, suggesting the power of 1/5. The above simple scaling analysis, the experiments,[17] and the stability criterion give 1/3. The formal origin of 1/5 power in thermal boundary layer theories is essentially similar to that in constant viscosity convection with rigid boundaries. For constant viscosity, the disagreement between the boundary layer theory and the experiments has been known for a long time: the boundary layer theory predicts 1/5 (see, e.g., Roberts[22]), while experiments give values which are closer to 1/3 rather than to 1/5 (see, e.g., Rossby[29]). A similar problem occurs in non-Newtonian viscosity convection as well (see below). This can be due to various reasons: the boundary layer solutions can be unstable, the aspect ratio can depend on the Rayleigh number and three-dimensional, time-dependent convection could be different from simple models usually considered (see also Ref. 30).

VII. NON-NEWTONIAN VISCOSITY CONVECTION

The scaling theory can be extended to non-Newtonian viscosity convection, although much less data are available in this case.

The viscosity law is supposed to be as follows:

$$\eta = \frac{b}{\tau_{II}^{n-1}}\exp(-\gamma T) = \frac{b^{1/n}}{e_{II}^{(n-1)/n}}\exp\left(-\frac{\gamma T}{n}\right), \tag{32}$$

where b, γ, and $n > 1$ are constants and $\tau_{II} = (\tau_{ij}^2/2)^{1/2}$ is the second invariant of the deviatoric stress tensor, and $\dot{e}_{II} = (\dot{e}_{ij}^2/2)^{1/2}$ is the second invariant of the strain rate tensor.

A. Small viscosity contrast regime

In the small viscosity contrast regime, the energy balance (5) is written as

$$\frac{b^{1/n}\exp(-\gamma T_i/n)}{(u_0/d)^{(n-1)/n}}\left(\frac{u_0}{d}\right)^2 V \sim \frac{\alpha g F}{c_p} V. \tag{33}$$

This can be interpreted as viscous dissipation (9) in a Newtonian fluid with an apparent viscosity

$$\eta_i \sim \frac{b^{1/n}}{(u_0/d)^{(n-1)/n}}\exp\left(-\frac{\gamma T_i}{n}\right) \tag{34}$$

calculated at the interior temperature $T_i \approx \Delta T/2$ and at the strain rate scale u_0/d.

The boundary layer equations (12) and (11) remain without changes.

We obtain

$$\delta_0 \sim \delta_1 \sim d Ra_n^{-n/(n+2)} = d Ra_0^{-(n-1)/(n+2)} Ra_i^{-1/(n+2)}, \tag{35}$$

where the Rayleigh numbers Ra_0, Ra_n and Ra_i are defined as follows:

$$Ra_0 = \frac{\alpha g \rho \Delta T d^{(n+2)/n}}{\kappa^{1/n} b^{1/n}}, \tag{36}$$

$$Ra_i = \frac{\alpha g \rho \Delta T d^{(n+2)/n}}{\kappa^{1/n} b^{1/n} \exp(-\gamma T_i)} = Ra_0 \, e^{\gamma T_i}, \tag{37}$$

$$Ra_n = \frac{\alpha g \rho \Delta T d^{(n+2)/n}}{\kappa^{1/n} b^{1/n} \exp(-\gamma T_i/n)} = Ra_0 \, e^{\gamma T_i/n}. \tag{38}$$

B. Transitional regime

In the transitional regime, the energy balance (5) is now written as

$$b \left(\frac{d^2 u_0}{\kappa \delta_0} \right)^{-(n-1)/n} \left(\frac{u_0}{\delta_0} \right)^2 \delta_0^2 l \sim \frac{1}{2} \frac{\alpha g F}{c_p} V, \tag{39}$$

which can be interpreted as viscous dissipation (16) in a Newtonian fluid with an apparent viscosity

$$\eta_0 \sim \frac{b^{1/n}}{(u_0/\delta_0)^{(n-1)/n}} \tag{40}$$

calculated at the surface temperature $T=0$ and at the strain rate scale u_0/δ_0. As in Newtonian viscosity convection, dissipation is assumed to be concentrated in the bend of the upper boundary layer with area of the order of δ_0^2.

The dissipation in the interior region is calculated in the same way as for the small viscosity contrast regime:

$$b e^{-\gamma T_i/n} \left(\frac{du_1}{\kappa} \right)^{-(n-1)/n} \left(\frac{u_1}{d} \right)^2 V \sim \frac{1}{2} \frac{\alpha g F}{c_p} V. \tag{41}$$

The results are as follows:

$$\delta_0 \sim d Ra_0^{-n/3}, \qquad \delta_1 \sim d Ra_0^{-(n^2+3n-3)/6(n+1)} Ra_i^{-1/2(n+1)}. \tag{42}$$

C. Stagnant lid regime

In the stagnant lid regime, dissipation in the central region is

$$b e^{-\gamma T_i/n} \left(\frac{du_1}{\kappa} \right)^{-(n-1)/n} \left(\frac{u_1}{d} \right)^2 V \sim \frac{\alpha g V}{c_p} F. \tag{43}$$

Convection beneath the lid is reduced to small viscosity contrast convection with an effective temperature difference scale (24). The following relations are obtained:

$$\delta_0 \sim d p^{2(n+1)/(n+2)} Ra_0^{-(n-1)/(n+2)} Ra_i^{-1/(n+2)}$$

$$= d p^{2(n+1)/(n+2)} Ra_n^{-n/(n+2)}, \tag{44}$$

$$\delta_1 \sim p^{-1} \delta_0. \tag{45}$$

Scaling laws for Newtonian viscosity convection in the stagnant lid regime can be obtained with the help of asymptotic boundary layer theories.[18,19] The problem can be treated analytically for non-Newtonian viscosity as well, provided the shear flow parallel to the bottom of the lid is dominant near the bottom of the lid (one of the main assumptions in boundary layer theories). With Morris and Canright's[18] assumption (see also Ref. 19) that the bottom of the lid is flat, we find

$$\delta_0 \sim d p^{3(n+1)/(2n+3)} Ra_n^{-n/(2n+3)}$$

$$= d p^{3(n+1)/(2n+3)} Ra_0^{-(n-1)/(2n+3)} Ra_i^{-1/(2n+3)}. \tag{46}$$

With Fowler's[19] assumption that the slope of the cold lid is of the order of δ_0/d (variations in the lid thickness are comparable with the lid thickness itself) we find

$$\delta_0 \sim d p Ra_n^{-n/(2n+3)} = d p Ra_0^{-(n-1)/(2n+3)} Ra_i^{-1/(2n+3)}, \tag{47}$$

which has a slightly different dependence on the parameter p compared to Eq. (46), both for Newtonian and non-Newtonian viscosity.

VIII. BOUNDARY LAYER STABILITY ANALYSIS: NON-NEWTONIAN VISCOSITY

As for Newtonian viscosity convection, it is useful to obtain scaling laws independently, based on the boundary layer stability analysis. Consider first onset of convection in a layer with the thickness d and with a strongly temperature-dependent viscosity fluid. As for Newtonian viscosity fluids,[24] we postulate that instability occurs in the sublayer with maximum Rayleigh number.

Such a sublayer must be located at the hot bottom, where the viscosity is smallest. The Rayleigh number for the sublayer is

$$Ra_{sub} = \frac{\alpha \rho g \nabla T z_{sub}^{2(n+1)/n}}{\kappa^{1/n} b^{1/n} \exp[-p(1-z_{sub}/2d)]}, \tag{48}$$

where z_{sub} is the thickness of the sublayer, $\nabla T = \Delta T/d$ is the temperature gradient in the layer and the effective viscosity is calculated at the mean temperature of the sublayer.

The requirement $\partial Ra_{sub}/\partial z_{sub} = 0$ gives the sublayer thickness at which the Rayleigh number is maximum:

$$z_{sub,m} = \frac{4(n+1)}{p} d. \tag{49}$$

If $p < 4(n+1)$, the maximum does not exist and instability occurs in the entire layer. If $p > 4(n+1)$, instability occurs in the sublayer. For $n=3$, it requires $e^p > e^{16} \approx 9 \times 10^6$, i.e., 3×10^3 larger than for Newtonian viscosity.

The onset of convection in the entire layer is determined by the onset of convection in this, the most unstable, sublayer:

$$Ra_{sub} = Ra_{cr}(n), \tag{50}$$

where $Ra_{cr}(n)$ is the critical Rayleigh number for a fluid whose non-Newtonian viscosity does not depend on temperature.

The criterion (50) can be written in terms of the critical Rayleigh number for the entire layer. This Rayleigh number is convenient to define at the bottom viscosity, as in the criterion (26) for Newtonian viscosity fluids:

$$Ra_1 = \frac{\alpha \rho g \Delta T d^{(n+2)/n}}{\kappa^{1/n} b^{1/n} \exp(-p/n)}. \tag{51}$$
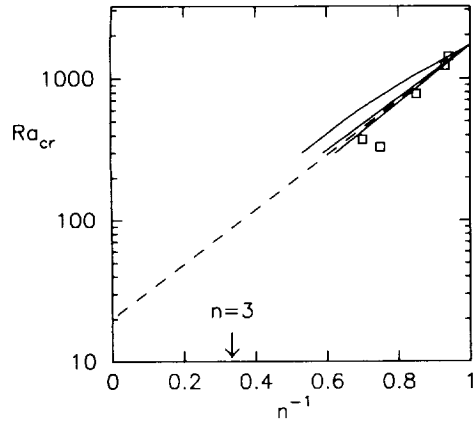
We obtain:

FIG. 5. The critical Rayleigh number for the onset of convection in power-law viscosity fluids is shown as a function of n^{-1}. Three solid curves correspond to various numerical calculations and the open boxes represent an experimental data set.[31,32] A linear extrapolation of all these data, Eq. (54), is indicated with a dashed line.

$$\mathrm{Ra}_{1,\mathrm{cr}} = \mathrm{Ra}_{\mathrm{cr}}(n) \left[\frac{e}{4(n+1)} \right]^{2(n+1)/n} p^{2(n+1)/n}. \qquad (52)$$

Assuming that the boundary layer is at the margin of convective stability, i.e.,

$$\frac{\alpha \rho g \Delta T \delta_0^{(n+2)/n}}{\kappa^{1/n} b^{1/n} \exp(-p/n)} = \mathrm{Ra}_{1,\mathrm{cr}}, \qquad (53)$$

we immediately obtain (44).

The critical Rayleigh number $\mathrm{Ra}_{\mathrm{cr}}(n)$ for non-Newtonian viscosity with no temperature dependence can be estimated using numerical and laboratory data.[31,32] For rigid boundaries, a linear extrapolation of those data suggest that (Fig. 5)

$$\mathrm{Ra}_{\mathrm{cr}}(n) \approx \mathrm{Ra}_{\mathrm{cr}}(1)^{1/n} \mathrm{Ra}_{\mathrm{cr}}(\infty)^{(n-1)/n}, \qquad (54)$$

where $\mathrm{Ra}_{\mathrm{cr}}(1) \approx 1708$ is the critical Rayleigh number for a constant viscosity fluid and $\mathrm{Ra}_{\mathrm{cr}}(\infty) \approx 20$ is the fitting coefficient corresponding to a formal asymptotic critical Rayleigh number in the limit $n \rightarrow \infty$. Assuming that the same functional form is approximately valid for the onset of convection in the sublayer, we use an exact value $\mathrm{Ra}_{\mathrm{cr}}(1) = 1568$ which is found numerically[24] for $n = 1$ and put $\mathrm{Ra}_{\mathrm{cr}}(\infty) \sim 20$ estimated above for rigid boundaries, the exact value of which does not substantially influence the results.

It is worth noting that the onset of convection in power-law fluids is always a finite amplitude instability because the viscosity depends on the amplitude of initial perturbations and goes to infinity when the perturbations approach zero. For such fluids, the meaning of the boundary between conductive and convective regimes (as implied in Refs. 31, 32 and in this section) is that if the Rayleigh number is below some critical value, no convective motion is possible with any initial conditions; if it is above this critical value, convection is possible but initiation of convection requires sufficiently large initial perturbations.

TABLE II. Theory versus experiments: Non-Newtonian viscosity $(n = 3)$.

Parameter	Theory	Fit
I. Small viscosity contrast regime		
δ_0	$\sim \mathrm{Ra}_0^{-0.4} \mathrm{Ra}_i^{-0.2}$	$2.0\mathrm{Ra}_0^{-0.38} \mathrm{Ra}_i^{-0.17}$
δ_1	$\sim \delta_0$	δ_0
u_0	$\sim \delta_0^{-2}$	$0.45\delta_0^{-2}$
ψ_m	$\sim \delta_1^{-2}$	$0.17\delta_1^{-2}$
II. Transitional regime		
δ_0	$\sim \mathrm{Ra}_0^{-1}$	$3.3\mathrm{Ra}_0^{-0.83}$
δ_1	$\sim \mathrm{Ra}_0^{-0.625} \mathrm{Ra}_i^{-0.125}$	$1.65\mathrm{Ra}_0^{-0.54} \mathrm{Ra}_i^{-0.092}$
u_0	$\sim \delta_0^{-2}$	$0.54\delta_0^{-2}$
ψ_m	$\sim \delta_1^{-2}$	$0.11\delta_1^{-2}$
III. Stagnant lid regime[a]		
δ_0	$\sim p^{1.6}\mathrm{Ra}_0^{-0.4} \mathrm{Ra}_i^{-0.2}$	$2.0p^{1.55}\mathrm{Ra}_0^{-0.38} \mathrm{Ra}_i^{-0.17}$
δ_1	$\sim p^{-1}\delta_0$	$p^{-1}\delta_0$
All regimes		
Nu	$(\delta_0 + \delta_1)^{-1}$	$(\delta_0 + \delta_1)^{-1}$
T	$(1 + \delta_1/\delta_0)^{-1}$	$(1 + \delta_1/\delta_0)^{-1}$

[a]In the absence of data, the "fit" uses the coefficients found in the small viscosity contrast regime.

IX. COMPARISON WITH EXPERIMENTS: NON-NEWTONIAN VISCOSITY

Christensen's[14] data are fitted with the help of equations presented in Table II and plotted in Fig. 6 together with the fitting curves for the first two regimes.
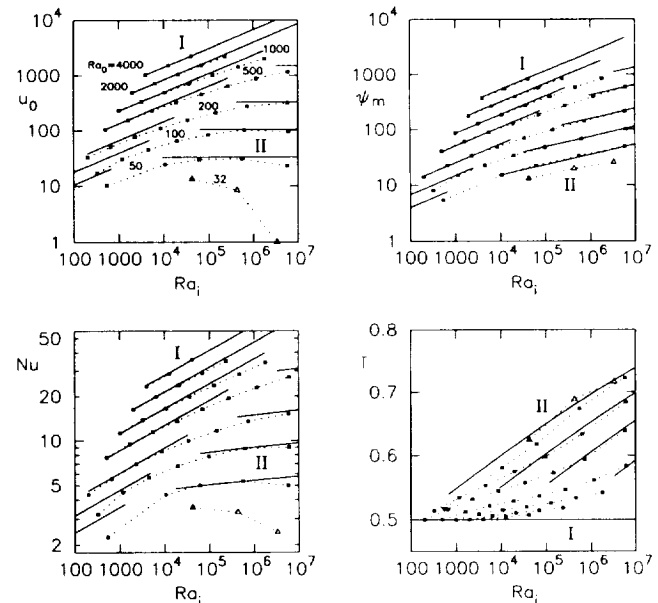

FIG. 6. The numerical[14] (solid boxes) and corresponding theoretical (solid lines) dependences of u_0, Nu, ψ_m, and T as functions of $\mathrm{Ra}_i \approx \mathrm{Ra}_i$ are shown for non-Newtonian $(n = 3)$ temperature-dependent viscosity convection. The Rayleigh number Ra_0 is fixed along each curve $(\mathrm{Ra}_0 = 50,100,250,500,1000,2000)$. Two convective regimes are: I—the small viscosity contrast regime and II—the transitional regime. The numerical data for $\mathrm{Ra}_0 = 32$ (triangles) do not obey the formulas suggested for these two regimes and, probably, indicate a transition to the third regime. This is shown in Fig. 7.